Reliable Low-Cost Fabrication of Low-Loss $Al_2O_3:Er^{3+}$ Waveguides With 5.4-dB Optical Gain

Kerstin Wörhoff, Jonathan D. B. Bradley, *Student Member, IEEE*, Feridun Ay, Dimitri Geskus, *Student Member, IEEE*, Tom P. Blauwendraat, and Markus Pollnau

***Abstract*—A reliable and reproducible deposition process for the fabrication of Al_2O_3 waveguides with losses as low as 0.1 dB/cm has been developed. The thin films are grown at ~ 5 nm/min deposition rate and exhibit excellent thickness uniformity within 1% over 50×50 mm^2 area and no detectable OH^- incorporation. For applications of the Al_2O_3 films in compact, integrated optical devices, a high-quality channel waveguide fabrication process is utilized. Planar and channel propagation losses as low as 0.1 and 0.2 dB/cm, respectively, are demonstrated. For the development of active integrated optical functions, the implementation of rare-earth-ion doping is investigated by cosputtering of erbium during the Al_2O_3 layer growth. Dopant levels between 0.2–5 $\times 10^{20}$ cm^{-3} are studied. At Er^{3+} concentrations of interest for optical amplification, a lifetime of the $^4I_{13/2}$ level as long as 7 ms is measured. Gain measurements over 6.4-cm propagation length in a 700-nm-thick $Al_2O_3:Er^{3+}$ channel waveguide result in net optical gain over a 41-nm-wide wavelength range between 1526–1567 nm with a maximum of 5.4 dB at 1533 nm.**

***Index Terms*—Aluminum oxide, erbium, integrated optics, low-loss dielectric waveguide, optical amplifier, reactive cosputtering.**

I. Introduction

AMORPHOUS aluminum oxide (Al_2O_3) doped with rare-earth ions is a very attractive material for active integrated optical (IO) applications such as amplifiers and lasers. The distinct advantages of dielectric waveguide lasers and amplifiers [1]–[3] over III–V technology are: potentially higher output powers as well as less noise and thermal drift. In the specific case of amorphous Al_2O_3, the feasibility of Si-compatible deposition with low fabrication complexity adds to the attractiveness. Moreover, the amorphous character of the host material results in emission linewidth broadening up to 55 nm around 1.55 μm [4]–[6], which is particularly important for amplifier applications in wavelength-division-multiplexing (WDM) devices and tunable laser sources. Last but not least, the relatively high refractive index, $n \sim 1.65$, allows for the realization of high-contrast channel waveguides with considerably more compact IO circuits compared to implanted waveguides [7], [8] or rare-earth-ion-doped fiber technology [9], [10].

During the past few decades, a number of research groups have investigated and developed Al_2O_3 deposition processes based on different techniques: pulsed laser deposition (PLD) [11], [12], atomic layer deposition (ALD) [13], [14], chemical vapor deposition (CVD) [5], [15]–[17], the sol-gel method [12], [18], [19], sputtering from a dielectric target [20], [21], and reactive cosputtering based on a metallic target [6], [22], [23].

Besides general requirements for thin-film applications in integrated optics, like low propagation loss, uniform growth over a large substrate area, good process reproducibility, and sufficiently high deposition rates, specific demands arising from applications in optically active devices need to be taken into account. For devices based on rare-earth-ion transitions, OH^--free deposition is required, because these bonds induce strong luminescence quenching and, hence, greatly diminish or prohibit optical gain. When comparing the properties of previously applied deposition techniques, it becomes obvious that CVD and sol-gel techniques inherently suffer from OH^- incorporation [5], [15], [16], [18] due to the presence of hydrogen in the process precursors. The application of ALD for optical waveguides, although resulting in thin films with excellent quality, is limited due to its very low deposition rate, which typically results in film thicknesses of only up to several tens of nanometers. The main drawback of PLD consists of the limited substrate area, typically 1–2 cm^2, which can be covered by a thin film with acceptable uniformity. This size limitation restricts the integration scale of complex IO devices. Based on the results of previous studies, the sputtering technique is very promising for the fabrication of amorphous Al_2O_3 thin films for integrated optics, since it combines an inherently low OH^- content with relatively fast, uniform, and controlled deposition over substrate areas of wafer scale.

Although the potential of rare-earth-ion-doped Al_2O_3 waveguides in IO amplifiers has been demonstrated by the achievement of 0.58-dB/cm net optical gain [24], breakthrough has been hampered by two problems: further loss reduction in slab and channel-type waveguides and the availability of a low-cost stable fabrication process. In planar Al_2O_3 waveguides, propagation losses of 0.23 dB/cm have been

Manuscript received July 03, 2008; revised October 27, 2008. Current version published April 03, 2009. This work was supported by the European Commission, EU-STREP 017501 "PI-OXIDE".

K. Wörhoff, J.D.B. Bradley, F. Ay, D. Geskus, and M. Pollnau are with the Integrated Optical Microsystems Group, MESA + Institute for Nanotechnology, University of Twente, 7500 AE Enschede, The Netherlands (e-mail: K.Worhoff@ewi.utwente.nl).

T.P. Blauwendraat was with the Integrated Optical Microsystems Group, MESA + Institute for Nanotechnology, University of Twente, 7500 AE Enschede, The Netherlands. He is now with OTB Solar, 5657 EB Eindhoven, The Netherlands.

Color versions of one or more of the figures in this paper are available online at http://ieeexplore.ieee.org.

Digital Object Identifier 10.1109/JQE.2009.2013365

reported for annealed thin films [21]. For the incorporation of rare-earth ions, an ion implantation process in combination with subsequent annealing has been applied [25], leading to increased fabrication complexity and cost. Exploiting reactive cosputtering based on dc-driven sputtering guns has resulted in as-deposited Al_2O_3:Er^{3+} waveguides with losses as low as 0.25 dB/cm for light propagating at 1.5-μm wavelength [6]. However, the main drawback of the applied method turned out to be the poor process stability and reproducibility, which was highly dependent on the condition of the sputtering target.

In this paper, the demonstration and optimization of reliable and highly stable deposition of rare-earth-ion-doped Al_2O_3 by reactive cosputtering will be presented, with an emphasis on the realization of as-deposited, low-loss optical waveguides. Incorporation of Er^{3+} into the optimized Al_2O_3 host material is studied in detail. Measurement results on dopant concentration, lifetimes, absorption and emission cross sections, and optical gain will be discussed.

II. Experimental

A. Waveguide Fabrication

1) Deposition Process: For the Al_2O_3 layer growth, an AJA ATC 1500 sputtering system equipped with a load-lock and three sputtering guns was applied. The sample was fixed in a bottom-up sputtering configuration on a substrate holder which can be rotated and heated up to a maximum temperature of 800 °C. The temperature was regulated within ± 3 °C. The deposition chamber can be pumped to a background pressure of 10^{-7} mTorr, which is essential in order to reach a negligible OH^- level in the deposition process. The pressure of the deposition process was adjusted by a valve with an accuracy of ± 0.1 mTorr. The three sputtering guns are designed for 2-in sputtering targets and can be driven individually by RF or dc power supplies, having a maximum range of 500 W. The power is set within ± 1 W. Flow-controlled Ar gas lines are connected to the sputtering guns. The Ar flow per gun is 100 sccm and can be controlled with an accuracy of 1%. In order to allow for oxide deposition from metallic targets (Al, Er), an oxygen (O_2) flow was added to the deposition process through a flow-controlled gas line which is connected to a gas inlet in the chamber wall. For the deposition of Al_2O_3 and doping with erbium, a high-purity Al target (99.999% purity) and a metallic Er target (99% purity) were mounted to the sputtering guns.

2) Channel Fabrication Process: Channel waveguides were fabricated by applying an Oxford Plasmalab 100 inductively coupled plasma (ICP) reactive ion etch system. The machine is equipped with a 3-kW ICP source and 600-W RF power supply connected to the substrate electrode. Both power supplies are driven by a 13.56-MHz generator. For the Al_2O_3 channel waveguide fabrication, a BCl_3-HBr etch process was applied. Process details are described elsewhere [26].

3) Sample Fabrication Procedure: Slab-type waveguides were fabricated by deposition of Al_2O_3 thin films on thermally oxidized 100-mm Si wafers. In order to ensure sufficient separation of the light propagating in the waveguide from the silicon substrate, 8-μm-thick thermal oxide was applied to all samples. Prior to deposition, all samples were cleaned by applying a standard cleaning process. After sample loading and substrate heating, temperature stabilization and target pre-sputtering for approximately 10 min was included in the deposition procedure. The sputtering time was adjusted for all depositions in order to grow waveguide layers within a typical thickness range of 0.5–1 μm. For the channel waveguide fabrication, standard lithography processes were applied after thoroughly cleaning the samples. The etch depth can be monitored *in situ* by an interferometric setup. After channel etching the residual resist was removed by oxygen plasma etching. The samples under investigation in this study have not been covered with a top cladding layer.

B. Structural Characterization

The thickness (d) and refractive index (n) of the layers were measured by a Woollam M44 spectroscopic ellipsometer and a Metricon 4-wavelength prism-coupling setup. The measurement accuracy of the presented thickness and refractive index values are below 0.5% and 5×10^{-4}, respectively. The nonuniformity of the layer thickness (δd) and the refractive index (Δn) over the wafer were measured by ellipsometry (Plasmos SD 2000) and prism coupling, respectively. From refractive index measurements utilizing TE and TM polarized light (prism coupling), the material birefringence given by $\Delta n_{\mathrm{TM-TE}} = n_{\mathrm{TM}} - n_{\mathrm{TE}}$ was calculated. The layer stress, which, in amorphous thin films, is known to be related to the material's birefringence, was measured by the wafer bow method. The stress values were calculated by combining data on the change in wafer bow over 80 mm, layer thickness, and substrate specific properties.

Composition and dopant concentration of the Al_2O_3:Er^{3+} films were measured by Rutherford back scattering (RBS) at the University of Utrecht. Samples of $\sim 10 \times 10$ mm^2 in size from the central part of the 100-mm wafers were prepared for measurements. The samples were exposed to a beam of 2.0-MeV He^+ ions with a current of 30 nA. The backscattered ions were detected under an angle of 170°. The sampled surface area was approximately 1 mm^2. The RBS spectra were evaluated by applying the RUMP software tool [27].

C. Optical Characterization

For optical loss measurements of slab-type waveguides, the moving prism method was applied. The measurement accuracy was ± 0.05 dB/cm. Absolute values of the optical loss were determined at fixed wavelengths based on laser sources at 633, 1320, and 1522 nm. Loss spectra were measured with 1-nm step size over a wide wavelength range of 500–1600 nm provided by a white-light source (Fianium supercontinum SC450), in combination with a spectrometer, and the spectral response was fitted to the absolute loss values obtained by the single-wavelength measurements. From baseline (background loss) corrected absorption peaks of the optical loss spectra and the measured Er^{3+} concentration, the absorption cross sections at several wavelengths (651, 795, 976, 1481, and 1529 nm) were determined.

The luminescence spectra were measured upon excitation with 150 mW (CW) at 977-nm wavelength from a Ti:sapphire laser. The light was prism-coupled. The luminescence was collected with a liquid optical fiber (Newport) and measured by

an optical spectrum analyzer (Spectro 320). From the luminescence spectra and the absorption cross sections, the emission cross sections were calculated. Lifetime measurements were carried out at the University of Hamburg. The luminescent decay curves at 1530 nm were measured upon excitation at 797 nm. Light from an optical parametric oscillator operating at 10-Hz repetition rate and 17-mJ pulse energy was focused onto the sample surface. The emitted light was collected, dispersed by a monochromator, and detected by a Ge photomultiplier (Hamamatsu H9170-75), which was connected to an oscilloscope for data acquisition.

For the measurement of small-signal gain, the samples were pumped at varying power (0–100 mW) from a Ti:sapphire laser operated at 977 nm. The low-power signal beam was tuned between 1480–1600 nm. Pump and signal beams were coupled simultaneously via a lens into the Er^{3+}-doped sample. In order to ensure good confinement of both beams when propagating through the sample, gain measurements were carried out in shallow-etched channel waveguides. Pump and signal light were chopped separately at different frequencies and the signal light was collected and measured by use of a lock-in amplifier. The amplification was determined by measuring the ratio of the amplifier output with pump on and off and the net gain was obtained after subtracting the measured absorption spectrum from the amplified signal over the investigated wavelength range.

III. Results and Discussion

A. Al_2O_3 Waveguide Fabrication

In order to optimize the Al_2O_3 deposition process towards reliable fabrication with high optical layer quality, the impact of processing parameters varied over a wide range (see Table I) on relevant layer properties (deposition rate R, refractive index n, film density ρ, stress σ, material birefringence $\Delta n_{\mathrm{TM-TE}}$, and optical loss α) was studied. Initially, both dc and RF-based sputtering were considered.

When comparing the dc and RF process, it becomes evident that the deposition rates of layers deposited by RF sputtering are typically a factor 2–4 lower than for dc-grown layers. In both cases, the deposition rate is mainly influenced by the sputtering power on the Al target, showing a nearly linear increase with power. Moreover, the difference in deposition rates of RF- and dc-grown layers becomes more pronounced at higher sputtering powers. The substrate temperature has hardly any impact on the deposition rate. Furthermore, the deposition rate decreases slightly at higher processing pressures and larger flow rates, which is connected to the impact of the decreased mean free path length of the species in the deposition chamber.

Compared to the dc-grown films the refractive index of the RF-grown layers is significantly higher. The difference is typically of the order of 3×10^{-2}. This rather large difference, which is nearly independent of the process parameter variations, can be explained by a particularity of the dc process: arcing on the sputtering target. This phenomenon is attributed to the oxidation of the target surface, resulting in the formation of an insulating layer and regular breakthrough (arcing) upon dc current application. With each arcing event, a large amount of clustered material is sputtered. Incorporation of such clusters in the thin film results in an increased amount of voids around those irregularities. This interpretation is supported by the film density measurements; the dc-grown layers have a significantly lower density.

TABLE I
Process Parameter Range for the Optimization Study of Al_2O_3 Layer Deposition Applying dc- and RF-Based Reactive Cosputtering

Parameter	DC process	RF process
Temperature T [°C]	400 - 500	350 - 650
Pressure p [mTorr]	3-5	3.5-6
Power P [W]	150 – 275	75 - 250
Total flow [sccm]	11 – 24.5	21 - 42
O_2 flow percentage [%]	10 - 25	5 – 10

When studying the change of refractive index upon process parameter variation, we observe the most significant impact when changing the chamber pressure; higher pressure results in a lower refractive index. This observation can be understood when considering an increased amount of collisions between species before reaching the sample surface, due to a decreased mean free path length in the case of deposition at higher pressures. These collisions increase the amount of gas phase reactions and formation of clusters, which are incorporated into the growing layer and result in a more porous, less dense structure. This finding is confirmed by the decrease of film density when grown at higher pressures.

The refractive index change upon variation of the other process parameters is less pronounced. Nevertheless, it yields information on the growth behavior, which becomes relevant when optimizing the deposition process towards highest film quality. Sputtering at powers below 200 W results in an increase of the refractive index with increasing power, whereas at higher power the refractive index remains nearly constant. The same trend is observed in the density measurements. This behavior can be understood when considering that, once the sputtered particles arrive at the sample surface, their kinetic energy is transformed to energy involved in the surface diffusion process. At low sputtering power the energy is too low to ensure sufficient surface mobility. At high sputtering powers further contribution of the kinetic energy to the surface diffusion process is most likely inhibited by the increased deposition rate.

An interesting observation was made for the refractive index and density change as a function of substrate temperature in the case of RF-grown layers. Based on the assumption of increased surface mobility at elevated substrate temperatures, one would expect thin films with increased refractive index and density when increasing the substrate temperature. From the measurements, however, a slight decrease of the refractive index was found at higher temperatures, while the density slightly increased. While the higher density is in line with the expectation of fewer voids at higher growth temperature, the refractive index response seems to be contradictory. However, when considering that the refractive index is not only determined by the film density but also by the material composition, this behavior

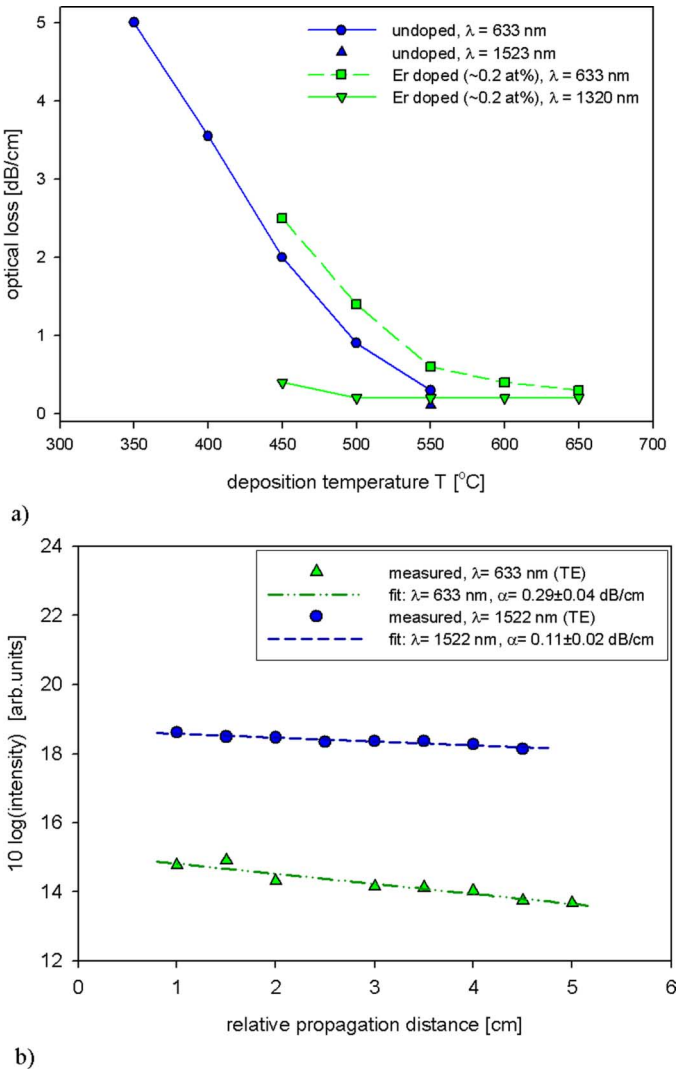

Fig. 1. (a) Optical losses of RF-sputtered Al_2O_3 waveguides as a function of deposition temperature. (b) Loss measurement of an as-deposited sample grown at optimized deposition parameters.

can be understood. The slightly lower refractive index indicates a more complete oxidation of the aluminum in the layer (less Al-Al bonds) at elevated temperatures. Since both voids in the film and incompletely oxidized Al result in higher losses in the shorter wavelength range, this interpretation is supported by the reduced optical losses of waveguides deposited by RF sputtering at higher temperatures [see Fig. 1(a)].

With respect to optical loss, we observed a significant difference between the dc and RF sputtering processes. While in the case of dc-grown layers light propagation failed, for the RF-grown layers, a clear dependence of the optical losses on the various process parameters was found. The main impact could be attributed to the substrate temperature. The losses decrease strongly as a function of temperature. Upon growth at 550 °C, the losses of as-deposited waveguides reach values as low as 0.29 ± 0.04 dB/cm and 0.11 ± 0.02 dB/cm at wavelengths of 633 and 1522 nm, respectively [see Fig. 1(b)]. Further loss reduction at higher temperatures is inconclusive, because the measurement limits of our setup were reached. In addition, the losses

TABLE II
LAYER PROPERTIES AT OPTIMIZED PROCESSING PARAMETERS FOR Al_2O_3 LAYERS BY REACTIVE COSPUTTERING

Layer property	value
Deposition rate *R* [nm/min]	5
Thickness uniformity [%] (6x6 cm^2 area)	± 1.4
Thickness reproducibility [%] (run-to-run)	± 4.5
Refractive index *n* at λ = 633 nm (TE)	1.659 ± 0.0005
Refractive index *n* at λ = 1550 nm (TE)	1.642 ± 0.0005
Material birefringence $\Delta n_{TE\text{-}TM}$	2 x 10^{-4}
Refractive index uniformity (6x6 cm^2 area)	± 2 x 10^{-4}
Refractive index reproducibility (run-to-run)	± 2 x 10^{-4}
Stress σ [MPa]	- 50 ± 5
Optical loss α [dB/cm]	0.3 (λ = 633 nm) 0.1 (λ = 1523 nm)

decrease slightly at lower flow rates and increase strongly in the high pressure range. These observations are in line with the fact that clusters and voids are included in the growing layer, as discussed above in connection with the behavior of refractive index and density as a function of processing pressure. A similar relationship between optical losses, refractive index, and density is also observed as a function of sputtering power. At low sputtering powers, where less dense layers with decreased refractive index are grown, the optical losses increase.

Based on the impact of processing parameters on the layer properties discussed above, the following optimized parameters have been chosen. The substrate temperature is kept at 550 °C; the sputtering power is 200 W; the total flow rate is 31.5 sccm with 5% oxygen addition; the chamber pressure is set at the lowest possible value at maximum pump capacity. Layer parameters of an Al_2O_3 waveguide, grown under optimized deposition conditions, were measured and are summarized in Table II. From the uniformity and reproducibility values as shown in the table, the high process stability becomes evident. Thickness and refractive index uniformity values of the Al_2O_3 sputtering process compare well with the uniformities obtained in Si-based CVD technologies [28]. As expected, the small birefringence is in line with the low values of tensile stress in the thin films.

B. Er^{3+}-Doped Waveguides

In order to investigate the growth behavior of Er^{3+}-doped Al_2O_3 layers, the RF power connected to the gun with the Er target was initially varied between 10–150 W. The remaining deposition parameters were kept at the values optimized for the Al_2O_3 deposition. The Er^{3+} concentration as obtained from RBS measurements is shown in Fig. 2. For Er cosputtering powers from 0 to 25 W, a nonlinearly increasing Er concentration was measured. At Er cosputtering powers above 25 W (not shown in Fig. 2), the concentration increases drastically. From the literature, it is known that concentrations near 1×10^{20} cm^{-3} are useful for amplification at 1.5 μm [24]. Er^{3+} concentrations between 2×10^{19} cm^{-3} and 4×10^{20} cm^{-3} can be achieved at sputtering powers between 10–25 W (see Fig. 2).

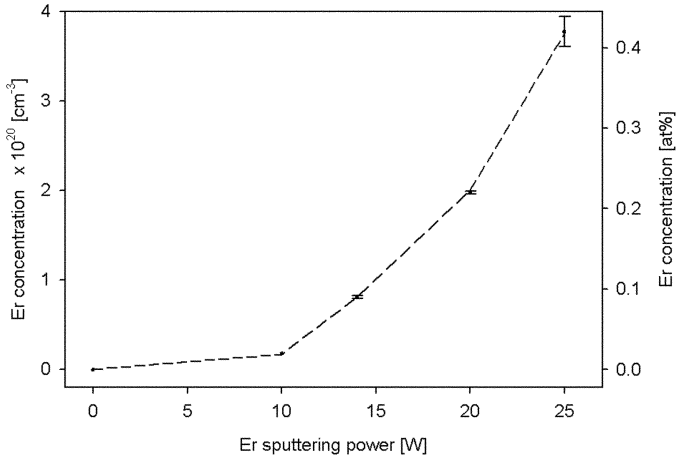

Fig. 2. Er^{3+} concentration of reactively cosputtered Al_2O_3:Er^{3+} as a function of sputtering power on the Er target.

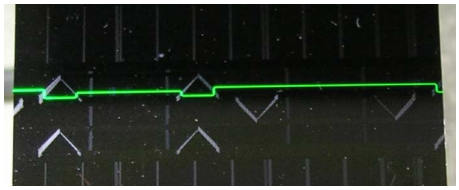

Fig. 3. Photograph of green upconversion observed in a bent Al_2O_3:Er^{3+} channel waveguide upon pumping at 976-nm wavelength.

In the following discussion on relevant spectroscopic properties of the active material, we will restrict ourselves to this range.

In the lower concentration range (2–8 $\times 10^{19}$ cm^{-3}), the luminescent lifetime $\tau_{\rm lum}$ of the 1535-nm emission ($^4I_{13/2} \rightarrow ^4I_{15/2}$) is of the order of 6.5–7.5 ms, which is comparable to values reported previously [4]. With increasing Er^{3+} concentrations, the lifetime decreases rapidly, which may be explained in part by impurity quenching owing to the low purity (99%) of the applied Er target and in part by energy-transfer upconversion, leading to green upconversion from the samples when pumped at 976-nm wavelength (Fig. 3). The intensity of the green upconversion light increases with the Er^{3+} concentration. An in-depth study of quenching and upconversion effects when applying higher purity targets will be subject to future research.

Absorption spectra were measured in the 500–1600-nm wavelength range for the samples grown under optimized deposition conditions with Er^{3+} concentrations varying between 2 $\times 10^{19}$ cm^{-3} and 4 $\times 10^{20}$ cm^{-3}. The absorption cross sections $\sigma^{\alpha}(\lambda)$ were calculated from the equation

$$\sigma^{\alpha}(\lambda) = \frac{\alpha_{\rm Er}(\lambda)}{10\log(e)\,\Gamma(\lambda)\,N_{\rm GS}} \tag{1}$$

where $\alpha_{\rm Er}(\lambda)$ is the absorption coefficient of the background-corrected Er^{3+} absorption peak at wavelength λ and $N_{\rm GS}$ is the population density of the ground state, which can be approximated by the Er^{3+} concentration $(N_{\rm Er})$ in the case of low excitation. $\Gamma(\lambda)$ expresses the confinement factor, which is given by the percentage of the beam intensity traveling at wavelength λ in the Er^{3+}-doped region. The absorption cross sections were calculated for the absorption peaks at the following wavelengths: 651 nm ($^4F_{9/2}$), 795 nm ($^4I_{9/2}$), 976 nm ($^4I_{11/2}$), 1481 nm ($^4I_{13/2}$), and the zero-phonon line at 1529 nm ($^4I_{13/2}$). The absorption cross sections determined in a sample with 8 $\times 10^{19}$ cm^{-3} Er^{3+} concentration are given in Table III. Comparison of the measured absorption cross sections with literature values shows good agreement.

TABLE III
COMPARISON OF ABSORPTION CROSS SECTIONS OF Al_2O_3:Er^{3+} WITH ABSORPTION PEAK WAVELENGTH IN BETWEEN PARENTHESES (THIS WORK: SAMPLE WITH 8 $\times 10^{19}$ cm^{-3} Er^{3+} CONCENTRATION)

ABSORPTION CROSS-SECTION (10^{-21} CM^2)					ref.
$^4F_{9/2}$	$^4I_{9/2}$	$^4I_{11/2}$	$^4I_{13/2}$	$^4I_{13/2}$	
4.03 (651 nm)	1.24 (795 nm)	1.63 (976 nm)	2.79 (1481 nm)	5.02 (1529 nm)	this work
			2.6 (1480 nm)	4.3 (1533 nm)	[6]
4.0 ± 0.7 (652 nm)	< 0.7 (not given)	1.7 ± 0.7 (980.5 nm)		5.7 ± 0.7 (1529 nm)	[30]
			2.7 (1480 nm)	5.8 (1530 nm)	[24]
			3.0 (1480 nm)	5.9 (1530 nm)	[25]

The emission spectrum of the $^4I_{13/2} \rightarrow ^4I_{15/2}$ transition was measured under 977-nm excitation. For a sample with an Er^{3+} concentration of $\sim 4\times 10^{20}$ cm^{-3}, the emission cross sections were calculated by two different methods. In McCumber's theory [29], the emission cross section $\sigma^e(\nu)$ as a function of photon energy $h\nu$ is derived from the absorption cross section $\sigma^a(\nu)$ as

$$\sigma^e(\nu) = \frac{Z_g}{Z_e}\exp\left(\frac{\varepsilon - h\nu}{kT}\right)\sigma^a(\nu) \tag{2}$$

where T is the temperature, k is Boltzmann's constant, and ϵ is the energy of the zero-phonon line. The partition functions of the excited (Z_e) and ground (Z_g) state can be approximated by $Z_g/Z_e \sim 1$. The assumption that the time to establish thermal equilibrium in each manifold is short compared to the lifetime of that manifold holds true for the $^4I_{13/2} \rightarrow ^4I_{15/2}$ transition in Al_2O_3:Er^{3+}.

The Füchtbauer–Ladenburg method [31] is based on the derivation of the emission cross section from the normalized shape of the photoluminescence spectrum $g(\nu)$ scaled by the radiative lifetime $\tau_{\rm rad}$:

$$\sigma^e(\nu) = \frac{\lambda^2}{8\pi n^2}\frac{1}{\tau_{\rm rad}}g(\nu) \tag{3}$$

where n is the refractive index of the Er^{3+}-doped waveguide layer. The radiative lifetime, which cannot be directly extracted from the measured luminescent lifetime due to deteriorating effects like quenching, was fitted in our approach such that the emission maximum at the zero-phonon line is calibrated.

The absorption and emission cross sections as a function of wavelength are shown in Fig. 4. As can be seen, the results of both methods are in fair agreement with each other. The emission cross section in the 1550–1560-nm wavelength range, being particularly interesting for active devices such as lasers, is

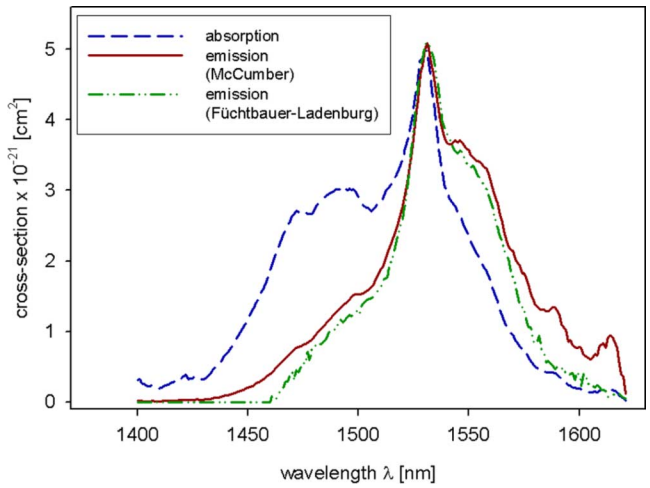

Fig. 4. Absorption and emission cross sections of an Er^{3+}-doped waveguide with $\sim 4 \times 10^{20}$ cm^{-3} Er^{3+} concentration.

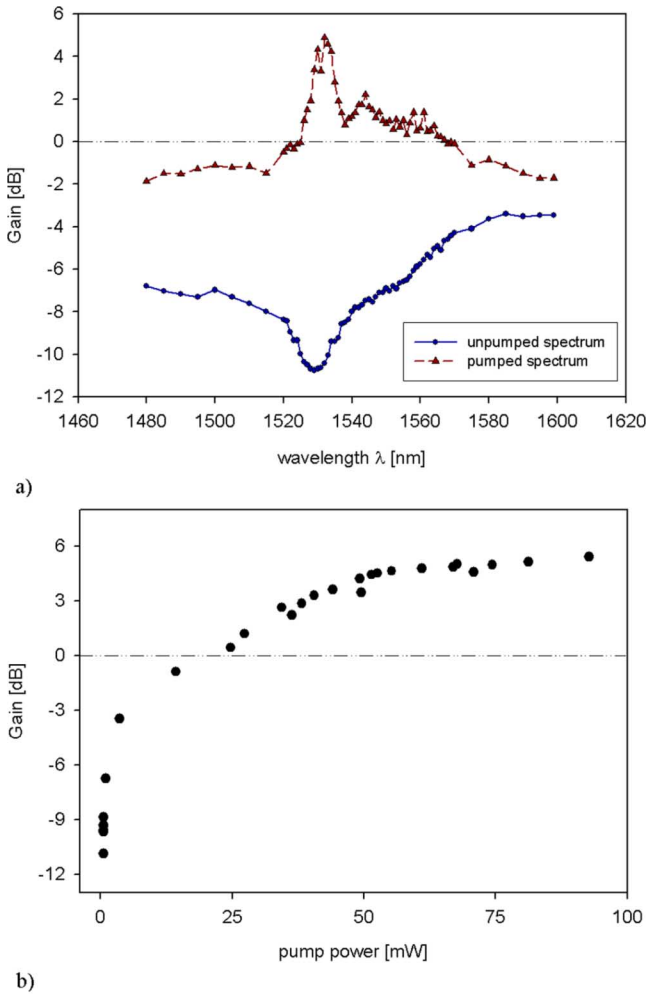

Fig. 5. (a) Gain spectrum of a sample with an Er^{3+} concentration of 9×10^{19} cm^{-3} pumped at 977 nm with 75 mW. (b) Signal amplification at 1533-nm wavelength versus pump power.

$3.3 \pm 0.2 \times 10^{-21}$ cm^2. The fitted radiative lifetime is 9.7 ± 0.5 ms and agrees well with previously reported values [6], [25].

C. Gain Measurements

For the gain measurements, shallow uncladded channel waveguides with an etch depth of ~ 20 nm were fabricated. Contrary to their planar counterparts, channel waveguides ensure tight confinement and excellent overlap of the pump and signal beams over several centimeters of propagation length in the waveguide layer. The gain spectrum was then obtained by subtracting the loss spectrum, which was measured in the planar waveguide previous to channel structuring, from the amplified signal spectrum. Channel waveguides with larger etch depth of 220 nm exhibited only slightly increased losses of 0.21 ± 0.05 dB/cm [26], compared to 0.11 ± 0.02 dB/cm in their planar counterparts, suggesting that in the shallow-etched channel waveguides applied in these gain experiments additional channel losses are negligible.

The spectral response of a 6.4-cm-long, 700-nm-thick Al_2O_3 waveguide with 9×10^{19} cm^{-3} Er^{3+} concentration is shown in Fig. 5(a). We obtained net optical gain over a 41-nm-wide wavelength range (1526–1567 nm). The gain was measured as a function of pump power (0–90 mW) after fixing the signal wavelength to the value of maximum amplification, 1533 nm [Fig. 5(b)]. From this graph, a gain threshold of 24 mW is extracted. The highest measured gain is 5.4 ± 0.2 dB at 90 mW pump power. In terms of gain per unit length, this results in 0.84 ± 0.03 dB/cm signal amplification. Although Er^{3+} concentration and channel waveguide geometry have as yet not been optimized, the measured gain value presents a significant improvement over the previously reported value of 0.57 dB/cm (2.9 dB over 4-cm length) [24].

IV. Conclusion

Al_2O_3 and Al_2O_3:Er^{3+} waveguides have been fabricated by a simple, reliable, and reproducible reactive cosputtering process and their fundamental optical and spectroscopic properties have been investigated. Planar and channel waveguides with losses as low as 0.1 and 0.2 dB/cm, respectively, and net optical gain over 41-nm spectral bandwidth with a maximum of 5.4 dB at 1533 nm have been demonstrated. In order to further improve the gain, a detailed investigation of the relevant upconversion and quenching processes and optimization of the Er^{3+} concentration appears to be necessary.

Based on these results, very compact integrated optical devices such as low-loss splitters and ring-resonators, high-speed amplifiers, integrated lasers, and the like become feasible. The fact that these devices will operate near 1550 nm and can be integrated directly on a silicon chip makes our approach especially attractive.

Acknowledgment

The authors would like to thank T. van Wijngaarden and W. A. Bik from the University of Utrecht for their support with the RBS measurements and A. Kahn, H. Scheife, and G. Huber from the University of Hamburg for their support with the lifetime measurement.

REFERENCES

[1] J. R. Lee, H. J. Baker, G. J. Friel, G. J. Hilton, and D. R. Hall, "High-average-power Nd:YAG planar waveguide laser that is face pumped by 10 laser diode bars," *Opt. Lett.*, vol. 27, no. 7, pp. 524–526, 2002.

[2] C. Grivas, D. P. Shepherd, T. C. May-Smith, R. W. Eason, and M. Pollnau, "Single-transverse-mode Ti:sapphire rib waveguide laser," *Opt. Exp.*, vol. 13, no. 1, pp. 210–215, 2005.

[3] Y. E. Romanyuk, C. N. Borca, M. Pollnau, S. Rivier, V. Petrov, and U. Griebner, "Yb-doped $KY(WO_4)_2$ planar waveguide laser," *Opt. Lett.*, vol. 31, no. 1, pp. 53–55, 2006.

[4] G. N. van de Hoven, E. Snoeks, A. Polman, J. W. M. van Uffelen, Y. S. Oei, and M. K. Smit, "Photoluminescence characterization of Er-implanted Al_2O_3 films," *Appl. Phys. Lett.*, vol. 62, no. 24, pp. 3065–3067, 1993.

[5] C. E. Chryssou and C. W. Pitt, "Er-doped Al_2O_3 thin films by plasma-enhanced chemical vapor deposition (PECVD) exhibiting a 55-nm optical bandwidth," *IEEE J. Quantum Electron.*, vol. 34, no. 2, pp. 282–285, Feb. 1998.

[6] S. Musa, H. J. van Weerden, T. H. Yau, and P. V. Lambeck, "Characteristics of Er-doped Al_2O_3 thin films deposited by reactive co-sputtering," *IEEE J. Quantum. Electron.*, vol. 36, no. 9, pp. 1089–1097, Sep. 2000.

[7] W. Sohler, B. K. Das, D. Dey, S. Reza, H. Suche, and R. Ricken, "Erbium-doped lithium niobate waveguide lasers," *IEICE Trans. Electron.*, vol. E88-C, no. 5, pp. 990–997, 2005.

[8] D. L. Veasey, D. S. Funk, P. M. Peters, N. A. Sanford, G. E. Obarski, N. Fontaine, M. Young, A. P. Peskin, W. C. Liu, S. N. Houde-Walter, and J. S. Hayden, "Yb/Er-codoped and Yb-doped waveguide lasers in phosphate glass," *J. Non-Cryst. Solids*, vol. 263–264, pp. 369–381, 2000.

[9] M. Yamada, H. Ono, T. Kanamori, S. Sudo, and Y. Ohishi, "Broadband and gain-flattened amplifier composed of a 1.55 mm-band and a 1.58 mm-band Er^{3+}-doped fibre amplifier in a parallel configuration," *Electron. Lett.*, vol. 33, no. 8, pp. 710–711, 1997.

[10] J. Hübner, P. Varming, and M. Kristensen, "Five wavelength DFB fiber laser source for WDM systems," *Electron. Lett.*, vol. 33, no. 2, pp. 139–140, 1997.

[11] A. Suarez-Garcia, J. Gonzalo, and C. N. Afonso, "Low-loss Al_2O_3 waveguides produced by pulsed laser deposition at room temperature," *Appl. Phys. A*, vol. 77, no. 6, pp. 779–83, 2003.

[12] A. Pillonnet, C. Garapon, C. Champeaux, C. Bovier, H. Jaffrezic, and J. Mugnier, "Fluorescence of Cr^{3+} doped alumina optical waveguides prepared by pulsed laser deposition and sol-gel method," *J. Lumin.*, vol. 87–89, pp. 1087–1089, 2000.

[13] Y. Kim, S. M. Lee, C. S. Park, S. I. Lee, and M. Y. Lee, "Substrate dependence on the optical properties of Al_2O_3 films grown by atomic layer deposition," *Appl. Phys. Lett.*, vol. 71, no. 25, pp. 3604–3606, 1997.

[14] S. Jakschik, U. Schroeder, T. Hecht, D. Krueger, G. Dollinger, A. Bergmaier, C. Luhmann, and J. W. Bartha, "Physical characterization of thin ALD-Al_2O_3 films," *Appl. Surf. Sci.*, vol. 211, no. 1-4, pp. 352–359, 2003.

[15] C. J. Kang, J. S. Chun, and W. J. Lee, "Properties of aluminum oxide films prepared by plasma-enhanced metal-organic chemical vapor deposition," *Thin Solid Films*, vol. 189, no. 1, pp. 161–173, 1990.

[16] M. Mahnke, S. Wiechmann, H. J. Heider, O. Blume, and J. Müller, "Aluminum oxide doped with erbium, titanium and chromium for active integrated optical applications," *Int. J. Electron. Commun.*, vol. 55, no. 5, pp. 342–348, 2001.

[17] X. Multone, C. N. Borca, and P. Hoffmann, "Large area deposition of Al_2O_3 thin films with molecular beams in high vacuum," *Thin Solid Films*, vol. 515, no. 19, pp. 7542–1745, 2007.

[18] M. Benatsou, B. Capoen, M. Bouazaoui, W. Tchana, and J. P. Vilcot, "Preparation and characterization of sol-gel derived Er^{3+}:Al_2O_3-SiO_2 planar waveguides," *Appl. Phys. Lett.*, vol. 71, no. 4, pp. 428–430, 1997.

[19] X. J. Wang and M. K. Lei, "Preparation and photoluminescence of Er^{3+}-doped Al_2O_3 films by sol-gel method," *Thin Solid Films*, vol. 476, no. 1, pp. 41–45, 2005.

[20] M. K. Smit, G. A. Acket, and C. J. van der Laan, "Al_2O_3 films for integrated optics," *Thin Solid Films*, vol. 138, no. 2, pp. 171–181, 1986.

[21] S. M. Arnold and B. E. Cole, "Ion beam sputter deposition of low loss Al_2O_3 films for integrated optics," *Thin Solid Films*, vol. 165, no. 1, pp. 1–9, 1988.

[22] B. J. H. Stadler, M. Oliviera, and L. O. Bouthillette, "Alumina thin films as optical waveguides," *J. Amer. Ceram. Soc.*, vol. 78, no. 12, pp. 3336–3344, 1995.

[23] Q. Song, C. R. Li, J. Y. Li, W. Y. Ding, S. F. Li, J. Xu, X. L. Deng, and C. L. Song, "Photoluminescence properties of the Yb:Er co-doped Al_2O_3 thin film fabricated by microwave ECR plasma source enhanced RF magnetron sputtering," *Opt. Mater.*, vol. 28, no. 12, pp. 1344–1349, 2006.

[24] G. N. van den Hoven, R. J. I. M. Koper, A. Polman, C. van Dam, K. W. M. van Uffelen, and M. K. Smit, "Net optical gain at 1.53 mm in Er-doped Al_2O_3 waveguides on silicon," *Appl. Phys. Lett.*, vol. 68, no. 14, pp. 1886–1888, 1996.

[25] G. N. van de Hoven, J. A. van de Elsken, A. Polman, C. van Dam, K. W. M. van Uffelen, and M. K. Smit, "Absorption and emission cross sections of Er^{3+} in Al_2O_3 waveguides," *Appl. Opt.*, vol. 36, no. 15, pp. 3338–3341, 1997.

[26] J. D. B. Bradley, F. Ay, K. Wörhoff, and M. Pollnau, "Fabrication of low-loss channel waveguides in Al_2O_3 and Y_2O_3 layers by inductively coupled plasma reactive ion etching," *Appl. Phys. B*, vol. 89, no. 2-3, pp. 311–318, 2007.

[27] RUMP Website [Online]. Available: http://www.genplot.com/doc/rump.htm

[28] K. Wörhoff, L. T. H. Hilderink, A. Driessen, and P. V. Lambeck, "Silicon oxynitride: a versatile material for integrated optics applications," *J. Electrochem. Soc.*, vol. 149, no. 8, pp. F85–F91, 2002.

[29] D. E. McCumber, "Einstein relations connecting broadband emission and absorption spectra," *Phys. Rev. A*, vol. 136, no. 4, pp. 954–957, 1964.

[30] C. Strohhöfer and A. Polman, "Absorption and emission spectroscopy in Er^{3+}-Yb^{3+} doped aluminum oxide waveguides," *Opt. Mater.*, vol. 21, no. 4, pp. 705–712, 2003.

[31] T. H. Hoekstra, "Erbium-doped Y_2O_3 integrated optical amplifiers," Ph.D. dissertation, Dept. Elect. Eng., University of Twente, Enschede, The Netherlands, 1994.

Kerstin Wörhoff received the M.Sc. degree in optoelectronics from the Technical University of Bratislava, Bratislava, Slovak Republic, in 1991 and the Ph.D. degree in applied physics from the University of Twente, Enschede, The Netherlands, in 1996.

In 1996, she joined the Lightwave Devices Group (now Integrated Optical MicroSystems Group, MESA + Institute for Nanotechnology), University of Twente, as a Postdoctoral Researcher. Since 2000, she has been an Assistant Professor with the same group. Her research interest covers the field of active and passive silicon-based photonics technology, rare-earth-ion doped devices, and integrated optical waveguide design. She has authored or coauthored more than 50 journal and conference papers and one patent.

Dr. Wörhoff is a member of the Electrochemical Society.

Jonathan D. B. Bradley (S'08) received the B.Eng. and M.A.Sc. degrees from McMaster University, Hamilton, ON, Canada, in 2003 and 2005, respectively. He is currently working toward the Ph.D. degree at the Integrated Optical MicroSystems Group, University of Twente, Enschede, The Netherlands.

His research interests include the design and fabrication of integrated optical devices, silicon-based photonics, and light emission and amplification in rare-earth-ion-doped dielectric materials.

Mr. Bradley is vice chair of the IEEE Lasers and Electro-Optics Society BENELUX student chapter.

Feridun Ay received the B.S. degree from the Middle East Technical University, Ankara, Turkey, in 1998 and the M.Sc. and Ph.D. degrees in 2000 and 2005, respectively, from Bilkent University, Ankara, Turkey, all in physics.

In 2005, he joined the Integrated Optical MicroSystems Group, MESA + Institute for Nanotechnology, University of Twente, Enschede, The Netherlands, as a Postdoctoral Researcher. His research interests include design and fabrication of active and passive waveguide components for applications in integrated optics. He has authored or coauthored more than 30 journal and conference papers.

Dr. Ay is a member of the European Physical Society and the Optical Society of America.

Dimitri Geskus (S'08) received the B.Sc degree from the Saxion Hogeschool, Enschede, The Netherlands, in 2003, and the M.Sc. degree from the University of Twente, Enschede, The Netherlands in 2006, both in applied physics. He is currently working toward the Ph.D. degree at the Integrated Optical MicroSystems Group, MESA + Institute for Nanotechnology), University of Twente.

His research is focused on integration of optical active devices in rare-earth-doped $KY(WO_4)_2$.

Mr. Geskus is treasurer of the IEEE Lasers and Electro-Optics Soceity BENELUX Student Chapter.

Tom P. Blauwendraat received the B.Sc. and M.Sc. degrees in applied physics from the University of Twente, Enschede, The Netherlands, in 2007. His thesis focused on Er-doped optical amplifiers.

He is currently with OTB Solar, Eindhoven, The Netherlands, as a Process Engineer for the industrial production of solar cells.

Markus Pollnau received the M.Sc. degree from the University of Hamburg, Hamburg, Germany, in 1992 and the Ph.D. degree from the University of Bern, Berne, Switzerland, in 1996, both in physics.

After postdoctoral positions with the University of Southampton and the University of Bern, he was a Project and Research Group Leader with the Swiss Federal Institute of Technology, Lausanne, Switzerland. In 2004, he was appointed a full Professor and chair of the Integrated Optical MicroSystems Group, University of Twente. He has contributed to more than 200 reviewed journal and international conference papers and six book chapters in the fields of crystal and thin-film growth, rare-earth-ion spectroscopy, solid-state and fiber lasers, and waveguide fabrication, devices, and applications. He has held European, Swiss, and Dutch personal fellowships and has obtained numerous national and European research grants. He has been involved in the organization of major international conferences, e.g., as Program (2006) and General (2008) Co-chair of the Conference on Lasers and Electro-Optics and as Program (2009) and General (2011) Co-chair of the Conference on Lasers and Electro-Optics Europe, and serves as Topical Editor for the *Journal of the Optical Society of America B*.

Prof. Pollnau is a member of the European Physical Society and the Optical Society of America.